Conformation Analysis

DOI: 10.1002/ange.200907143

Tracking Flavin Conformations in Protein Crystal Structures with Raman Spectroscopy and QM/MM Calculations**

*Åsmund Kjendseth Røhr, Hans-Petter Hersleth, and K. Kristoffer Andersson**

Flavin cofactors are among the most efficient and flexible electron carriers involved in cell metabolism. Incorporated in a protein framework they can operate as redox mediators between two-electron donors and one-electron-acceptor molecules, perform various catalytic reactions, and act as molecular switches in light-activated cell-signaling processes.[1–3] The isoalloxazine unit of flavins is able to adopt different redox and protonation states, as represented in Scheme 1 by the oxidized flavin mononucleotide FMN, anionic semiquinone $FMN^{\bullet-}$, neutral semiquinone $FMNH^{\bullet}$, and anionic hydroquinone $FMNH^{-}$.

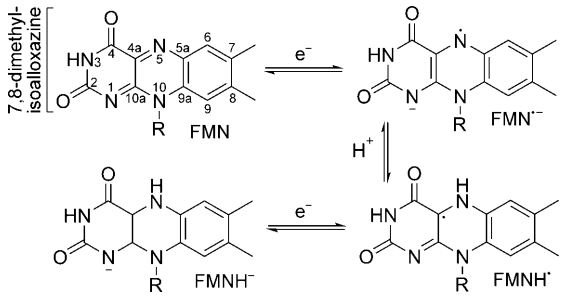

Scheme 1. Selected physiologically relevant FMN redox and protonation states (R = ribityl phosphate).

The versatility in chemical behavior is thought to originate from the conformational interplay between a protein and the flavin cofactor, which affects its environment through electrostatic interactions, bending of the isoalloxazine moiety, aromatic stacking with amino acid side chains, and the formation of hydrogen bonds, depending on its redox and protonation state.[4–6] The analysis of more than 1000 protein 3D structures deposited in the protein data bank (PDB) that contain the flavin cofactors FMN or flavin dinucleotide (FAD) showed that the dihedral angle between the planes formed by the pyrimidine and benzene rings of the isoalloxazine moiety, also referred to as the "butterfly bend", varies from 0 to 34°.[7] However, a straightforward correlation between the flavin structure, as determined by X-ray crystal-structure analysis, and its molecular function can be deceptive. The intense X-rays generate photoelectrons that can reduce active-site cofactors of the protein during X-ray crystal-data collection[8,9] and thus change the flavin geometry. As a result, flavin redox states and structures may be misinterpreted. This phenomenon has been recognized for flavins;[10–12] however, there has been no detailed assessment of the extent to which intense X-rays lead to structural alterations of the flavin moieties. Knowledge of these processes and the proper tools that can be used to resolve these challenges is necessary to enhance our understanding of flavin functionality.

Herein, we present structures obtained at atomic resolution of the FMN-containing flavoenzyme NrdI in its initial oxidized form ($NrdI_{ox}$) and neutral semiquinone form ($NrdI_{sq}$). The X-ray crystallographic analysis was complemented by in situ single-crystal Raman spectroscopy to determine the active-site structure with respect to its redox and protonation state, whereby spectra were recorded prior to and subsequent to X-ray crystal-data collection. The experimental flavin geometries were also modeled through quantum-mechanical/molecular-mechanical (QM/MM) calculations. With this study, we aimed to shed light on the extent of flavin-cofactor perturbation due to experimental setup and to construct more accurate models of the enzyme active site with the flavin cofactor in various redox and protonation states.

The *Bacillus cereus* NrdI enzyme (Figure 1) belongs to a group of enzymes that are thought to be important for the in vivo function of class Ib ribonucleotide reductase (RNR). These enzymes reduce the diferric oxygen-bridged metal cluster of the R2 subunit to the diferrous state and thus initiate the regeneration of the essential tyrosyl radical.[13–15] The crystal structures of $NrdI_{ox}$ and $NrdI_{sq}$ were refined to a resolution of 1.12 and 1.15 Å, respectively. During refinement, no restraints were applied to the planarity or bond lengths of the FMN cofactor (Figure 2a). The chemical reduction of the $NrdI_{ox}$ crystal to $NrdI_{sq}$ before crystallographic data collection was confirmed by single-crystal Raman spectroscopy (Figure 2b) and light-absorption spectroscopy (see Figure S1b in the Supporting Information).

Single-crystal Raman spectroscopy has previously been used to probe the buried and solvent-exposed conformations of the flavin cofactor in flavodoxin and *para*-hydroxybenzoate

[*] Å. K. Røhr, Dr. H.-P. Hersleth, Prof. Dr. K. K. Andersson
Department of Molecular Biosciences, University of Oslo
0316 Oslo (Norway)
Fax: (+47) 2285-6041
E-mail: k.k.andersson@imbv.uio.no
Homepage: http://folk.uio.no/~KKAN

[**] This research was supported by the Steering Board for Molecular Life Sciences at the University of Oslo (EMBIO) and the Norwegian Research Council (grants 177661V30 and 138370V30; synchrotron-related research in the Oslo region, SYGOR). We thank the team at the Swiss–Norwegian Beamline (BM01) at the ESRF for their valuable help. We also thank Dr. Giorgio Zoppellaro for helpful discussions. QM/MM = quantum mechanical/molecular mechanical.

Supporting information for this article is available on the WWW under http://dx.doi.org/10.1002/anie.200907143.

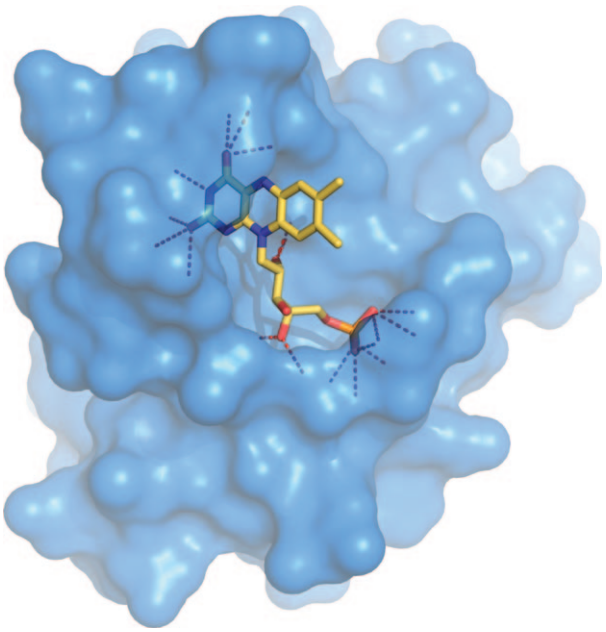

Figure 1. View of the FMN cofactor (yellow) bound in a pocket on the NrdI surface. The benzene ring of the isoalloxazine moiety is solvent-exposed, whereas the pyrimidine ring is buried and hydrogen-bonded to the protein. The dashed red lines represent polar contacts with distances less than 3 Å.

hydroxylase;[16,17] however, to our knowledge no such experiments have been combined with X-ray crystallography. The isoalloxazine ring system of our frozen NrdI crystals exhibited a number of sharp Raman bands that are characteristic of flavin proteins in the 1100–1800 cm^{-1} region (Tables 1 and 2).[18] The Raman spectra were obtained with a diode laser with an excitation wavelength of 785 nm (BM01, ESRF). The Raman bands of the $NrdI_{ox}$ and $NrdI_{sq}$ crystals before exposure to X-rays were assigned on the basis of hybrid density functional theory (DFT) calculations of lumiflavin (7,8,10-trimethylisoalloxazine; the frequencies were scaled by a factor 0.9614[19]) in combination with reported assignments of flavin Raman modes.[20–22]

Table 1: Comparison of Raman shifts for $NrdI_{ox}$ before and after X-ray crystal-data collection.

$\tilde{\nu}_{before}$ [cm^{-1}][a]	$\tilde{\nu}_{calcd}$ [cm^{-1}][b]	Assignment[c]	$\tilde{\nu}_{after}$ [cm^{-1}][d]
1720	1716	ν(C4=O), δ(N3–H)	
1665	1698	ν(C2=O), δ(N3–H)	
1609	1609	ν(ring I)	1609
1582	1566	ν(N5–C4a), ν(C10a–N1)	
1549	1528	ν(ring I), ν(C10a–N1)	
1501	1515	ν(N5–C4a), ν(C10a–N1), ν(ring I)	
1466	1473	ν(ring I,II), methyl deformation	1476
1408	1408	ν(ring I,II), methyl deformation	1401
1357	1324	a) ν(ring I,II,III)	
	1350	b) δ(N3–H)	
	1354	c) ν(ring I,II,III), δ(N3–H)	
1229	1239	δ(C6–H), δ(C9–H)	1234

[a] Raman bands recorded for single-crystal NrdI flavin before X-ray crystal-data collection. [b] Raman shifts calculated by using UB3LYP, 6-31+G(d,p). [c] Approximate stretching (ν) and bending (δ) modes. [d] Raman bands observed in the spectrum recorded after X-ray crystal-data collection.

Table 2: Comparison of Raman shifts for $NrdI_{sq}$ before and after X-ray crystal-data collection.

$\tilde{\nu}_{before}$ [cm^{-1}][a]	$\tilde{\nu}_{calcd}$ [cm^{-1}][b]	Assignment[c]	After X-ray irradiation[d]
1666	1683	ν(C2=O), δ(N3–H)	n.c.
	1649	ν(C4=O), δ(N3–H)	
1617	1592	ν(ring I)	n.c.
1609	1582	ν(ring I), δ(N5–H), ν(C10a–N1), ν(N5–C4a)	n.c.
1531	1683	ν(C10a–N1), ν(ring I), δ(N5–H)	d.i.
1505	1649	δ(N5–H), ν(ring I,II)	d.i.
1397	1592	ν(ring I), ν(N5–C4a), ν(C10a–N1)	d.i.
1345	1582	δ(N5–H), δ(N3–H), ν(ring I,II,III)	d.i.
1231	1683	δ(N5–H), δ(C6–H), δ(C9–H)	d.i.

[a–c] See Table 1. [d] Raman bands are indicated for which no apparent change (n.c.) or an approximate 50% decrease in intensity (d.i.) was observed after X-ray crystal-data collection.

The single-crystal Raman spectra of $NrdI_{ox}$ and $NrdI_{sq}$ (Figure 2b) showed that the flavin structure (and hence the vibrational modes) changed during X-ray crystal-data collection. The influence of X-ray radiation was most apparent for oxidized FMN crystals: in the spectra of these crystals, a number of bands shifted in frequency or disappeared, and an increase in fluorescence from the crystal was observed. The diminishment of the carbonyl stretching vibration at 1720 cm^{-1} can be rationalized by comparing the calculated frequencies of this vibration in the oxidized and one-electron-reduced anionic semiquinone lumiflavin models: the difference in frequency is 78 cm^{-1}. Raman bands at 1582, 1549, and 1501 cm^{-1} are dominated by vibrations involving the N5, C4a, C10a, and N1 atoms; the corresponding bond lengths depend on the flavin redox state. These Raman modes also disappeared upon X-ray illumination. Additionally, the peak positions of some modes described mostly by ring stretching, hydrogen-atom bending, and methyl deformation changed by a few wavenumbers.

For crystals soaked in sodium dithionite to generate the neutral semiquinone form of FMN, the intensity of the flavin Raman bands decreased after X-ray irradiation (Figure 2b). The fluorescence from the crystal also decreased substantially. These observations indicate the conversion of the neutral semiquinone form into the fully reduced anionic form $FMNH^-$, which is a poor Raman scatterer.[23]

With the aim of describing radiation-induced perturbations of and protein effects on isoalloxazine geometries, we modeled different redox and protonation states of the flexible flavin cofactor in a frozen protein environment by using QM/MM methods. Previously, ab initio calculations of lumiflavin (LF) in physiologically relevant protonation states in vacuo predicted approximately planar structures for the oxidized and one-electron-reduced semiquinone isoalloxazine ring systems, whereas the two-electron-reduced hydroquinone

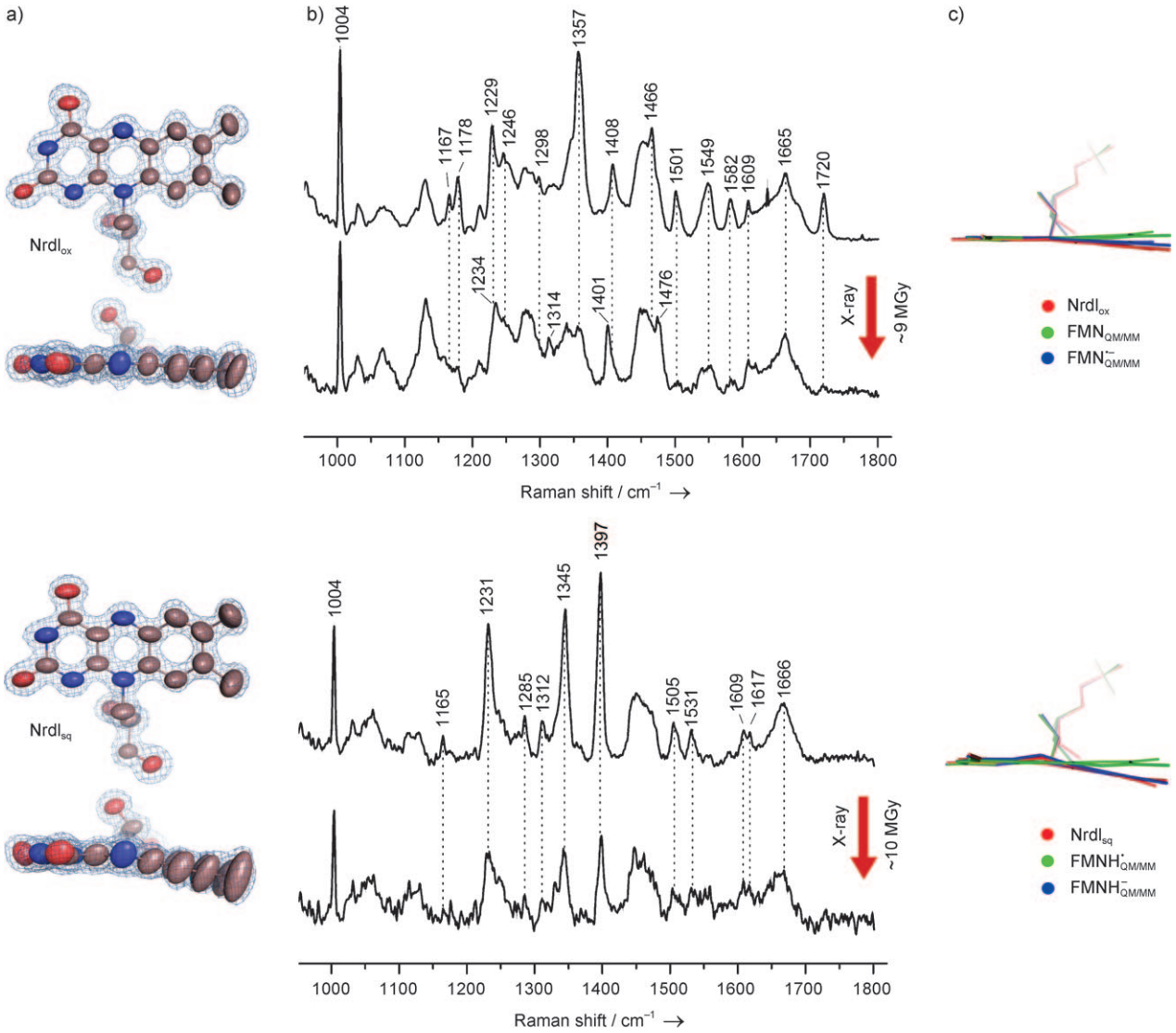

Figure 2. a) Ellipsoids drawn at 50% probability describing atomic-displacement parameters of the NrdI flavin cofactors enclosed by the σ_A-weighted $2F_o-F_c$ map contoured at 1 σ. b) In situ single-crystal Raman spectra of NrdI before and after data collection with the cofactor initially in its oxidized state (PDBid:2X2O) and neutral semiquinone state (PDBid:2X2P). c) Comparison of experimental structures with QM/MM models. The one-electron-reduced flavin models (blue) correspond to the experimental structures (red), whereas the models of the initial systems are essentially planar (green).

forms are bent around the virtual N5–N10 axis.[24] The corresponding bending angles observed in NrdI$_{ox}$ and NrdI$_{sq}$ deviate from planarity by 4.6 and 11.0°, respectively: a significant distortion in comparison to the theoretical predictions. The B3LYP hybrid functional was used for the isoalloxazine ring system and most of the connected ribityl chain, whereas the AMBER force field was applied to the protein scaffold and FMN remnants. We used the protein structure of NrdI$_{ox}$ when modeling the oxidized FMN and one-electron-reduced FMN$^{\bullet-}$ states. When NrdI$_{ox}$ is chemically reduced to NrdI$_{sq}$, the isoalloxazine N5 atom becomes protonated and forms a hydrogen bond to the protein backbone, which undergoes a conformational change (see Figure S2 in the Supporting Information). Consequently, we used the NrdI$_{sq}$ crystal structure when modeling the protonated, reduced states FMNH$^{\bullet}$, FMNH^{-}, and FMNH$_2$.

The crystal structures of the FMN cofactors of NrdI$_{ox}$ and NrdI$_{sq}$ are shown in Figure 2a; the atoms are displayed as ellipsoids describing the experimental atomic displacement parameters (ADPs). From these representations, it can be seen that the benzene part of the isoalloxazine unit exhibit disorder perpendicular to the molecular plane. If the changes in the Raman spectra are taken into account, it is most likely that these ADPs are a record of the structural distortion accumulated during X-ray crystal-data collection and not a result of molecular flexibility. The effect is most pronounced for NrdI$_{sq}$, which indicates that the largest shift from the initial state occurs in this structure. Strikingly, the QM/MM models that most accurately resemble the experimental structures NrdI$_{ox}$ and NrdI$_{sq}$ are those which correspond to the one-electron-reduced forms of the oxidized and semiquinone flavins, FMN$^{\bullet-}{}_{QM/MM}$ and FMNH$^{-}{}_{QM/MM}$, respectively (Fig-

ure 2c and Table 3). The oxidized and neutral semiquinone models $FMN_{QM/MM}$ and $FMNH^{\bullet}_{QM/MM}$ both have a propeller twist along the length of the isoalloxazine moiety and are

Table 3: Comparison of experimental structures with QM/MM and hybrid DFT geometry-optimized models.

	RMSD [Å][a]		Butterfly bend [°][b]
	$NrdI_{ox}$	$NrdI_{sq}$	
$FMN_{QM/MM}$[c]	0.115		−3.1 (−7.7)
$FMN^{\bullet-}_{QM/MM}$	**0.075**		**3.3 (−1.3)**
LF_{B3LYP}	0.085		0.0 (−4.6)
$LF^{\bullet-}_{B3LYP}$	0.086		0.0 (−4.6)
$FMNH^{\bullet}_{QM/MM}$[c]		0.171	−3.9 (−14.9)
$FMNH^{-}_{QM/MM}$		**0.075**	**14.1 (+3.1)**
$LFH^{\bullet}_{B3LYP}$		0.161	0.0 (−11.0)
LFH^{-}_{B3LYP}		0.123	19.5 (+8.5)
$FMNH_{2\ QM/MM}$[c]	0.204	0.270	−7.1
$LFH_{2\ B3LYP}$	0.307	0.230	26.1

[a] Root-mean-square deviation of the geometry-optimized model from the experimental X-ray crystal structure. [b] Dihedral angle of the two isoalloxazine planes defined by the virtual N5–10 axis. Values in parenthesis are the difference with respect to the corresponding experimental structure. [c] The isoalloxazine ring system is propeller-twisted rather than bent.

slightly bent in the opposite direction with respect to the experimental structures. Hence, these models are influenced by the protein environment and deviate from the corresponding planar lumiflavin (LF) models, which were geometry-optimized in vacuo.

To conclude, we have shown in this study how X-ray crystallography, which is used as a method for determining the structure of proteins, itself induces structural changes in the flavin moiety. We have demonstrated the value of in situ Raman spectroscopy and QM/MM calculations for the accurate interpretation of the structure of the active site in flavin proteins. In our model system, the flavin cofactors of both $NrdI_{ox}$ and $NrdI_{sq}$ crystal structures are most correctly described as the intermediate radiation-induced one-electron-reduced states of FMN and $FMNH^{\bullet}$, respectively. As mentioned earlier, the butterfly bending of flavins has been linked to reactivity, the tuning of redox potential, and signal transduction. Therefore, the many flavoprotein crystal structures deposited in the Protein Data Bank that have been determined without monitoring by in situ spectroscopy have to be treated with caution if used to deduce detailed reaction mechanisms on the basis of their flavin structures.

Received: December 18, 2009
Published online: February 24, 2010

Keywords: cofactors · enzymes · molecular modeling · Raman spectroscopy · structural biology

[1] V. Massey, *Biochem. Soc. Trans.* **2000**, *28*, 283–296.
[2] E. B. Purcell, S. Crosson, *Curr. Opin. Microbiol.* **2008**, *11*, 168–178.
[3] E. Demarsy, C. Fankhauser, *Curr. Opin. Plant Biol.* **2009**, *12*, 69–74.
[4] M. Senda, S. Kishigami, S. Kimura, M. Fukuda, T. Ishida, T. Senda, *J. Mol. Biol.* **2007**, *373*, 382–400.
[5] Y. T. Kao, C. Saxena, T. F. He, L. J. Guo, L. J. Wang, A. Sancar, D. P. Zhong, *J. Am. Chem. Soc.* **2008**, *130*, 13132–13139.
[6] N. Lostao, C. Gómez-Moreno, S. G. Mayhew, J. Sancho, *Biochemistry* **1997**, *36*, 14334–14344.
[7] T. Senda, M. Senda, S. Kimura, T. Ishida, *Antioxid. Redox Signaling* **2009**, *11*, 1741–1766.
[8] O. Carugo, K. D. Carugo, *Trends Biochem. Sci.* **2005**, *30*, 213–219.
[9] H.-P. Hersleth, Y. W. Hsiao, U. Ryde, C. H. Gorbitz, K. K. Andersson, *Biochem. J.* **2008**, *412*, 257–264.
[10] D. S. Berkholz, H. R. Faber, S. N. Savvides, P. A. Karplus, *J. Mol. Biol.* **2008**, *382*, 371–384.
[11] R. Kort, H. Komori, S. Adachi, K. Miki, A. Eker, *Acta Crystallogr. Sect. D* **2004**, *60*, 1205–1213.
[12] A. Mees, T. Klar, P. Gnau, U. Hennecke, A. P. M. Eker, T. Carell, L. O. Essen, *Science* **2004**, *306*, 1789–1793.
[13] I. Roca, E. Torrents, M. Sahlin, I. Gibert, B. M. Sjoberg, *J. Bacteriol.* **2008**, *190*, 4849–4858.
[14] J. A. Cotruvo, J. Stubbe, *Proc. Natl. Acad. Sci. USA* **2008**, *105*, 14383–14388.
[15] M. Kolberg, K. R. Strand, P. Graff, K. K. Andersson, *Biochim. Biophys. Acta Proteins Proteomics* **2004**, *1699*, 1–34.
[16] A. J. W. G. Visser, L. A. Carreira, J. Legall, J. Lee, *J. Phys. Chem.* **1980**, *84*, 3344–3346.
[17] M. D. Altose, Y. G. Zheng, J. Dong, B. A. Palfey, P. R. Carey, *Proc. Natl. Acad. Sci. USA* **2001**, *98*, 3006–3011.
[18] A. J. W. G. Visser, J. Vervoort, D. J. Okane, J. Lee, L. A. Carreira, *Eur. J. Biochem.* **1983**, *131*, 639–645.
[19] A. P. Scott, L. Radom, *J. Phys. Chem.* **1996**, *100*, 16502–16513.
[20] Y. G. Zheng, J. Dong, B. A. Palfey, P. R. Carey, *Biochemistry* **1999**, *38*, 16727–16732.
[21] S. Kikuchi, M. Unno, K. Zikihara, S. Tokutomi, S. Yamauchi, *J. Phys. Chem. B* **2009**, *113*, 2913–2921.
[22] D. H. Murgida, E. Schleicher, A. Bacher, G. Richter, P. Hildebrandt, *J. Raman Spectrosc.* **2001**, *32*, 551–556.
[23] Y. G. Zheng, P. R. Carey, B. A. Palfey, *J. Raman Spectrosc.* **2004**, *35*, 521–524.
[24] Y. J. Zheng, R. L. Ornstein, *J. Am. Chem. Soc.* **1996**, *118*, 9402–9408.

